Vietnam Journal of Science and Technology ***63*** *(4) (2025) 745-756*
doi:10.15625/2525-2518/17636

Isothermal oxidation property of plasma sprayed 20YSZ/NiAl thermal barrier coating

Pham Thi Ly[1, *], Nguyen Van Tuan[1], Nguyen Tuan Anh[1], Pham Thi Ha[1], Dao Bich Thuy[1], Ly Quoc Cuong[1], Vo An Quan[1], Le Hai Dang[2]

[1]*Institute of Materials Science, Vietnam Academy of Science and Technology, 18 Hoang Quoc Viet, Nghia Do, Ha Noi, Viet Nam*

[2]*Chemistry Faculty, Hanoi National University of Education, 136, Xuan Thuy, Cau Giay, Ha Noi, Viet Nam*

[*]Email: *lypham09.nd@gmail.com*

Received: 4 November 2022; Accepted for publication: 29 March 2023

Abstract. In this study, 20 wt.% yttria-stabilized zirconia (20YSZ) thermal barrier coatings (TBCs) were deposited by air plasma spraying (APS) on 310S stainless steel with NiAl as a bond coat. The TBCs were exposed to an isothermal oxidation test in an electric furnace under the air at 1000 ^{o}C for 8, 24, 48, 120, and 200 hours. Thermal oxidation characteristic of the coating was evaluated through cross-sectional structure, phase composition, and tensile adhesive strength. Results show that the 20YSZ coating consisted of mainly a thermodynamically stable cubic phase (Arkalite). The porosity, the thickness of the thermal growth oxide (TGO) layer, and the adhesive strength of the research sample had changes depending on the time of the isothermal oxidation. After exposure at 1000 ^{o}C, the porosity of the coating could be reduced by up to 62.3 % compared to the initial coating; the adhesion strength was improved significantly. The TGO thickness was high, but its growth rate tended to slow down and stabilize for the isothermal oxidation duration in a range of 24 ÷ 200 hours.

Keywords: YSZ, thermal barrier coating, oxidation property, TGO growth, porosity.

Classification numbers: 2.5.3, 2.9.1, 2.9.2.

1. INTRODUCTION

Thermal barrier coatings (TBCs) are widely applied in protecting metallic components, which are used in aero- and land-based gas turbines. For more than four decades, yttria-stabilized zirconia (YSZ) has been used successfully as a top coat in TBCs due to its outstanding material properties [1].

The YSZ plasma coating has good thermal stability and a high melting point (about 2700 ^{o}C). It is one of the lowest thermal conductivity coatings among high-temperature ceramic coatings [2]. The coefficient of thermal expansion of this coating is 11 × 10^{-6} K^{-1} [3]. In addition, the thermal conductivity of YSZ block and YSZ coating with different structures and porosity are 2.6 W/mK (5.3 wt.% YSZ, 600 ^{o}C) and 0.7 ÷ 1.4 W/mK (7.25 wt.% YSZ), respectively [4, 5].

In insulation coating applications, the YSZ coating is often deposited with a metallic coating that acts as a bonding layer, which is usually composed of MCrAlY (M = Ni or Co). The YSZ coating has a characteristic rough surface of coatings made by plasma spray coating. Roughness depends on the particle size of the material, its molten state, and the dynamics of impact. The YSZ structure is heterogeneous, and the particle size in the coating is also very diverse, ranging from nanometers to micrometers [6]. The typical porosity of the YSZ plasma coating is in the range of 10 ÷ 20 % [7, 8]. Pores in the coating can be divided into three types with different orientations and shapes, such as intralayer cracks, interlayer voids, and spherical voids [9, 10]. The existence of pores degrades the mechanical properties of the material and alters the failure mechanism of TBCs [11 - 13]. However, it is possible to improve the porosity of the coating through some measures, such as adjusting spray parameters, sintering, and sealing [14, 15].

The structure of YSZ coating after the isothermal oxidation process consists of three components, such as YSZ ceramic coating (top coat), metal coating (bond coat), and thermal growth oxide (TGO) layer - an oxidized scale can be formed on the bond coat during thermal cycling due to the diffusion of oxygen through the ceramic coating towards the bond coat. The TGO layer has the main function of protecting the substrate from oxidation [2]. However, this increase in the TGO thickness is related to the expansion volume in an enclosed space at the interface of the bond coat and YSZ layer leading to the development of compressive stress [16, 17]. When this value reaches the critical 10 - 15 μm, the TBCs system can be degraded [18, 19]. Therefore, besides performing tests on mechanical properties and coating structure, the assessment of the TGO growth during the isothermal oxidation time is widely used in many studies [20 - 22].

The 8YSZ (ZrO_2 - 8 wt.% Y_2O_3) material has been most habitually used for plasma-sprayed TBCs, so most of the research literature has focused on the plasma-sprayed 8YSZ coating. However, in comparison with the 8YSZ coating, the 20YSZ (ZrO_2 - 20 wt.% Y_2O_3) coating has lower porosity and exits with a thermodynamically stable cubic phase [22]. For this reason, in the study, the isothermal oxidation property of the 20YSZ plasma coating system was investigated.

2. EXPERIMENTAL PROCEDURE

2.1. Material preparation

Table 1. Chemical composition of the 310S substrate.

Element	C	Si	S	P	Mn	Ni	Cr	Mo
%wt	0.0462	0.6239	0.0016	0.0233	11.852	20.2283	25.7674	0.0089
Element	V	Cu	W	Ti	Sn	Co	Al	Fe
%wt	0.0536	0.0170	0.0045	0.0059	0.0020	0.2372	0.0218	51.733

The 310S stainless steel (Jay Jagdamba Co., Ltd, India) with the chemical composition listed in Table 1 was used as the substrate in this research. The substrate was cut into samples with a size of 50 × 50 × 5 mm and specially designed according to the drawing in Figure 1 for adhesion testing. The 20YSZ powder (ZrO_2- 20 wt.% Y_2O_3) was used as the main part of the top

coat and the NiAl (5 wt.% Al) as the bond coat. These powders were provided by Wisdom Co., Ltd (China). Before deposition, the powders were sieved to ensure uniform particle size in the range of 30 ÷ 100 µm.

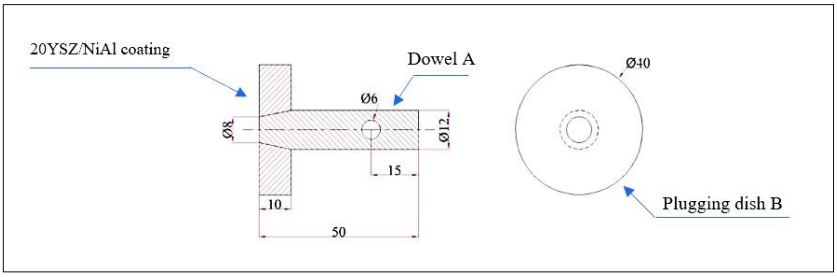

Figure 1. Drawing of the adhesion test specimen.

2.2. Preparation of plasma sprayed coating

After sand blasting of the substrate by use of Al_2O_3 corundum abrasive particles with a size of 0.8 ÷ 1.2 mm, a NiAl bond coat with a thickness of 100 µm was applied on the substrate surface by the air plasma spraying (APS) method using PRAXAIR-TAFA plasma-spraying machine. Then, the coating of 20YSZ with a thickness of 300 µm was applied on the bond coat surface. The APS parameters for the coatings are presented in Table 2.

Table 2. Plasma-spraying operating parameters.

Spray Parameters	**NiAl Bond coat**	**20YSZ Top coat**
Plasma current, A	425	530
Primary gas Ar, Psi	60	60
Secondary gas H_2, Psi	15	15
Spray angle	90^o	90^o
Spray distance, mm	80	80
Powder feed rate, g/min	19	16
Powder carry gas Ar, Psi	40	40

2.3. Oxidation test

The 20YSZ specimens were subjected to isothermal oxidation testing at 1000 °C for a holding duration of 8, 24, 48, 120, and 200 hours inside an electric furnace with a heating rate of 3 °C/min in an air atmosphere. After each oxidation time, the 20YSZ specimens were cooled to ambient temperature in the furnace and were investigated for their characteristics.

2.4. Research methods

The cross-section microstructure and the TGO thickness were examined using a scanning electron microscope SM-6510LV (Japan). The porosity of the 20YSZ coating was obtained from SEM images magnified 500 times by using the image analysis method, so it represented the

macroscopic porosity of the evaluated coating. The XRD analysis was performed using a Panalytical Empyrean diffractometer (Poland) with Cu-Kα radiation, 2θ angle scanning from 10^o to 70^o, and a step width of 0.03^o. The adhesion of the coating samples was determined by the dowel pull method using Shimadzu equipment (Japan). The dowel A was pulled out of the plugging dish B with a speed of 20 mm/min. The adhesion force was recorded when the sample was broken.

3. RESULTS AND DISCUSSION

3.1. Cross-sectional structure of the coating

Figure 2 shows the cross-sectional images of the 20YSZ coating sample taken by a scanning electron microscope. As can be observed in Figure 2, both of 20YSZ top coat and NiAl bond coat had typical characteristics of thermal spraying by the APS technique, including lamellar structure, globular pores, and microcracks.

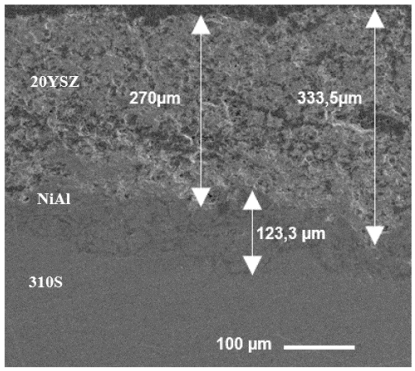

Figure 2. SEM cross-sectional image of the 20YSZ coating sample (×150).

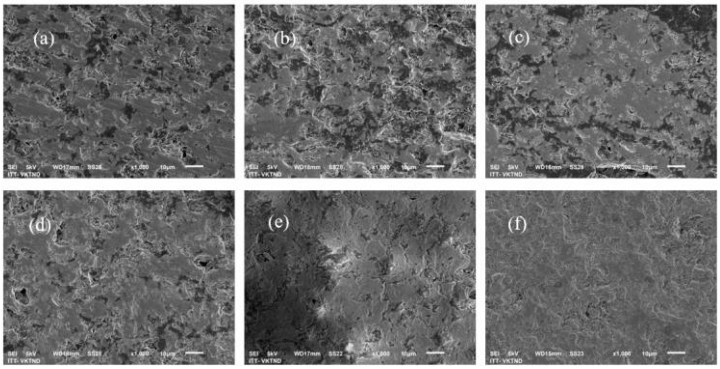

Figure 3. The cross-sectional SEM images of the 20YSZ coating: as sprayed (a), after exposing at 1000 ˚C for exposure times of 8 (b), 24 (c), 48 (d), 120 (e), and 200 hours (f).

For the 20YSZ coating, the cross-sectional SEM images (Figure 3) show that after 8 hours and 24 hours of thermal oxidation at 1000 ^{o}C, the structure of the coating had an insignificant change from the as-sprayed coating. The remaining porosity is clearly observed in the SEM images. However, when the exposing time was increased to 48 hours, the sintering process made the coating structure denser. The structural image of 20YSZ coating after the holding time at 1000 ^{o}C of 200 hours had a dramatic difference compared to the as-sprayed coating with the disappearing pores in the coating.

For the interface between the bond coat and the ceramic top coat, the SEM images (Figure 4) indicate that the NiAl coating was oxidized in the high-temperature environment to form the TGO layer. The TGO thickness of the investigated coatings at each oxidation cycle was also measured by quantitative SEM image analysis. The growth of the TGO layer versus the time of oxidation at 1000°C is presented in Figure 5. As a result, the lowest TGO thickness of about 53.6 µm was recorded in the sample after the thermal oxidation time of 8 hours and the highest value was about 90.2 µm recorded in the sample after the thermal oxidation duration of 200 hours. Thus, the TGO thickness increased with increasing the thermal oxidation time. However, in the first stage of the oxidation from 8 hours to 24 hours, the rate of growth of the TGO layer was faster than in the later stage from 24 hours to 200 hours. This phenomenon can be explained

that in the first stage of the thermal oxidation process, the porosity of the 20YSZ coating was relatively large, so oxygen could easily diffuse through the pores of the ceramic coating toward the bond coat. When extending thermal exposure time, the path of oxygen transportation in this coating had been decreased by the reducing porosity due to the sintering process, and therefore, the TGO thickness also increased at a less rate [20].

Although the thickness of the TGO layer was relatively high, the 20YSZ coatings had not been destroyed after the exposure at 1000 ^{o}C for 200 hours.

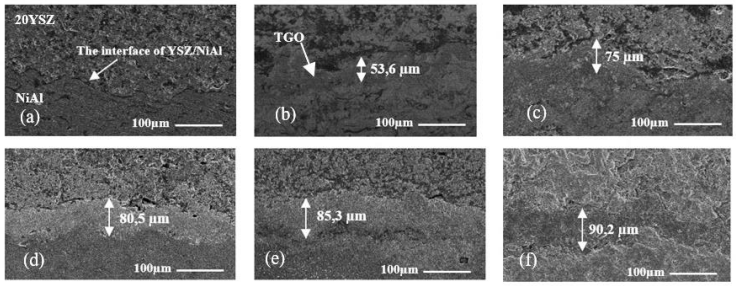

Figure 4. The cross-sectional SEM images of the samples at the interface of top coat/bond coat: as-sprayed (a), after exposing at 1000 ˚C for exposure times of 8 (b), 24 (c), 48 (d), 120 (e), and 200 hours (f).

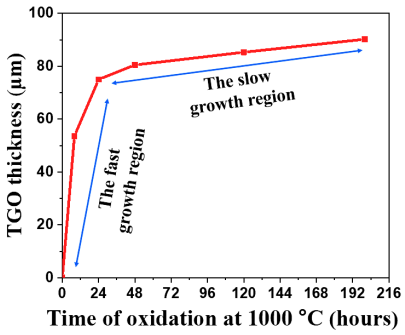

Figure 5. The growth of the TGO layer versus time of oxidation at 1000 °C.

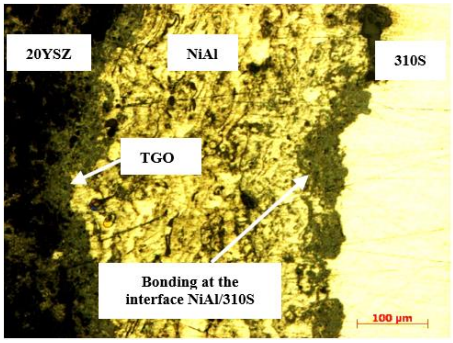

Figure 6. The structure of the 20YSZ coating sample after exposure at 1000 ^{o}C for 8 hours.

For the NiAl bond coat, after being deposited by the high energy of the plasma spraying and undergoing the oxidation process at 1000 ^{o}C, the microstructure of the coating was extremely dense. In addition, the image at the interface of the NiAl bond coat and the steel substrate before and after the thermal exposing cycle also proves the bonding formation between this coating and the substrate since the exposing time at 1000 ^{o}C was 8 hours. Figure 6 is the structure image of the 20YSZ coating sample after exposure at 1000 °C for 8 hours which was taken by an optical microscope.

3.2. Porosity of the coating

SEM images with x500 magnification were used to obtain the porosity of the coating samples, so these porosity values represent the macroscopic porosity of the coating [23]. The porosity of 20YSZ coating samples over time of the isothermal oxidation at 1000 ^{o}C are shown in Figure 7.

As can be observed in Figure 7, the initial 20YSZ coating had a high porosity (about 26 %) and tended to decrease continuously during the isothermal oxidation testing at 1000 ^{o}C. The reason is that during the high-temperature service procedure, the granules in the coating grow because of sintering. The grain-boundary grooving through the thermal diffusion phenomena causes the pore surface to become rougher, and then bridges for atom diffusion are formed between the lamellae interfaces that connect to the inter-splat pores. Thus, by the time, these pores eventually close, and the microstructure of the coating densifies [23]. After 200 hours of the isothermal oxidation, the porosity of the 20YSZ coating reached 9.8 % which decreased by about 62.3 % in comparison with the as-sprayed coating, but the reduction rate of the porosity value had not shown any signs of stabilization. Normally, the porosity reduction rate of the YSZ coating is slower and more stable when a holding time at high temperatures is longer than 200 hours [22, 24].

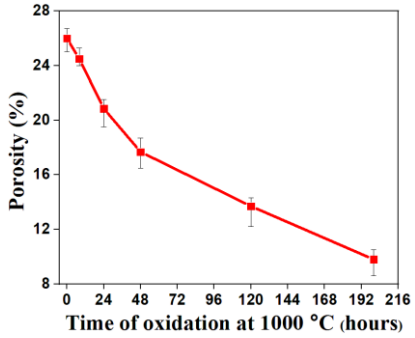

Figure 7. The porosity values of the 20YSZ coating versus time of oxidation at 1000 °C.

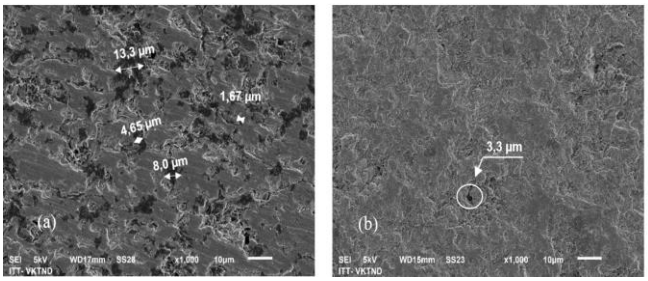

Figure 8. The pore size of 20YSZ coating before (a) and after exposing at 1000 ^{o}C for 200 hours (b).

The porosity of the 20YSZ coating not only directly affects the TGO thickness but also affects the thermal insulation ability of the coating. However, these two dimensions of influence have opposite meanings. The reduction of porosity in the 20YSZ coating decreases the TGO thickness, which can be beneficial in ensuring a stable structure for the coating system. According to what was previously mentioned, the thermal growth oxide (TGO) layer is an oxidized scale that can be formed on the bond coat during thermal cycling due to the diffusion of oxygen through the pores of the ceramic coating towards the bond coat. The increase in the TGO thickness is related to the expansion volume in an enclosed space at the interface between the bond coat and YSZ layer leading to the development of residual compressive stress [16, 17]. If the porosity is too high, the TGO will grow rapidly which causes increasing the compressive stress in the coating. As a result, the TBCs system can be degraded [18, 19]. Therefore, reducing of the TGO thickness by decreasing the coating's porosity can contribute to enhancing the quality of the coating system. In contrast, the excessive reduction of porosity increases the thermal conductivity of the coating because the total disappearance or significant volume reduction of the pores is equivalent to the building-up strongly of new bondings between lamellae splats in the coating. This is the main reason for the increase in the ability to transfer heat of the coating. Studies have shown that the thermal conductivity of YSZ plasma coatings can be increased by about 100 ÷ 150 % due to the reduction of porosity during sintering [23]. This behavior significantly decreases the performance of the TBC system in the service condition in high-temperature environments. Thus, the 20YSZ coating needs to have suitable porosity to achieve both of these goals.

Besides porosity, pore size is also a factor to consider. Coating samples with too small pores size will be rapidly healed by the sintering process, leading to a decrease in porosity and an increase in thermal conductivity. The pores whose width is less than 100 nm may disappear after a few hours of sintering at high temperatures due to their high surface energy and nanoscale width [25, 26]. In this study, the 20YSZ initial coating consists of pores with a relatively large width which can be up to 13.3 µm. After the thermal oxidation testing, the pore size decreases, leading to a decrease in the porosity of the coating. After holding at 1000 ^{o}C for 200 hours, the pores with small sizes were filled, the remaining pores had the largest size of about 3.3 µm. Figure 8 shows the pore size of 20YSZ coating before and after exposure at 1000 ^{o}C for 200 hours.

3.3. Phase composition of the coating

Figure 9 shows the XRD patterns of the 20YSZ coatings before and after high-temperature exposure. On the X-ray diffraction pattern, there are nickel metal, arkelite (ZrO_2), and bunsenite (NiO) phases. All three of these crystalline phases have a cubic structure.

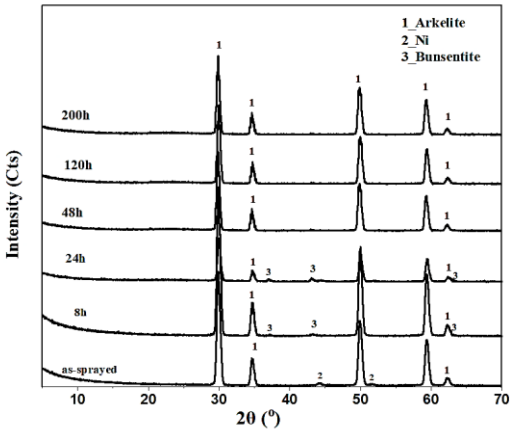

Figure 9. The XRD patterns of the 20YSZ coating versus time of oxidation at 1000 °C.

The as-sprayed 20YSZ coating sample presented mainly arkelite and nickel phases. Upon the high-temperature exposure for 8 hours and 24 hours, on the XRD pattern, there was the appearance of bunsenite, instead of the diffraction peak of nickel. It indicates that the Ni was oxidized to form NiO which was the main component of the TGO layer. However, when increasing the thermal oxidation time, the diffraction peak of bunsenite disappeared, although this crystalline phase always survived in the coating samples. The proof is that the green color of NiO was still easily detected at the interface between the 20YSZ and NiAl coatings where occurred the failure in the adhesion test (Figure 11). The reason may be that the denser 20YSZ coating structure during the isothermal oxidation test prevented the diffraction signal of this crystalline phase.

The arkelite crystal phase, which is the main component of the 20YSZ coating, is a ZrO_2 compound with a cubic structure. This phase structure did not undergo any further change during plasma spraying and after the high-temperature exposure at 1000 ^{o}C for 200 hours. The XRD results of both the 20YSZ spray powder and the coating samples contained the arkelite phase only. The phase transition temperature of the ZrO_2 cubic phase is 2370 °C, which is higher than that of the tetragonal and monoclinic phase (> 1150 °C) [27]. In addition, the ZrO_2 cubic and

tetragonal phases also have a higher density than the monoclinic phase [28]. The structural stabilization of the ZrO_2 cubic phase during the isothermal oxidation test at 1000 ^oC helped stabilize the material volume, resulting in no additional formation of compressive stress in the 20YSZ internal coating. Moreover, the ZrO_2 cubic phase has low thermal conductivity and chemical stability over a wide high-temperature range [29]. These contributed to ensuring the 20YSZ coating system in this study might be durable in high-temperature environments and responded to the standard of a thermal barrier coating.

3.4. Adhesion testing of the coatings

The coating samples with different oxidation times had different types of fracture in the adhesion test, mainly with two types of failure simulated in Figure 10. Figure 11 is the image of the dowel's head of the samples.

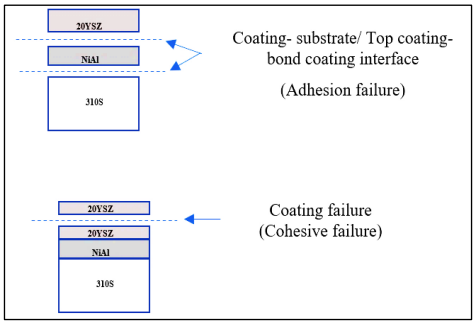

Figure 10. Types of failure resulting from adhesion testing of the coatings.

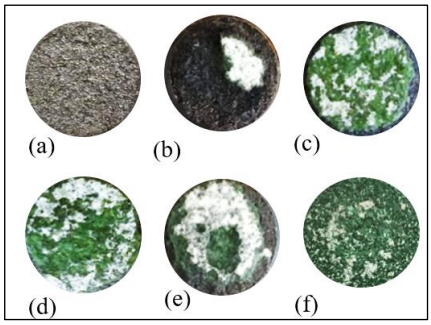

Figure 11. Image of the dowel's head after adhesion testing: as sprayed (a), after exposing at 1000 ˚C for exposure times of 8 (b), 24 (c), 48 (d), 120 (e), and 200 hours (f).

As can be seen in Figure 11, the 20YSZ as-sprayed coating sample exhibited adhesion failure with the fractured position being at the interface of the steel substrate and the NiAl bond coat. After holding at 1000 ^oC for 8 hours, the fractured position was still at the interface of the steel substrate and the NiAl bond coat, but the peeling area was reduced compared to the as-sprayed coating sample. It can be explained that after 8 hours of heat treatment, the bonding between the NiAl bond coat and the 310S steel substrate formed at some positions as seen in Figure 6. When expanding the isothermal oxidation time, the boundary region between the NiAl and 20YSZ coatings became the weakest bonding position of the samples. All three samples exposed at 1000 ^oC for 24, 48, and 120 hours presented both adhesive failure at the interface of the two coatings and cohesive failure with a part of the 20YSZ coating being separated. However, when the thermal oxidation time of 200 hours, the internal bonding force of the 20YZS coating was enhanced because of its dense structure, so the cohesive failure in the 20YZS coating did not happen. There was only a fracture at the interface of the two coatings. Thus, the formation of the TGO layer during the oxidation test reduced the adhesion strength between the NiAl coating and the 20YSZ coating. However, the exposure to the high temperature might also contribute to increasing the adhesion of the NiAl bond coat and the 310S steel substrate due to the appearance of the bonding region. The adhesive strength results in Table 3 and Figure 12 are also consistent with the above statements.

The results in Table 3 and Figure 12 show that the average adhesion strength of the 20YSZ as-sprayed coating sample was about 12.53 MPa which was 2 ÷ 3 times lower than that of the

exposed samples at 1000°C. Besides, the coating samples with different oxidation times had different adhesion strength values. Among these specimens, the coating sample held at 1000°C for 8 hours exhibited the best adhesion strength (about 38.52 MPa). The remaining samples presented adhesion strength in the range of 24.5 ÷ 29 MPa. Thus, in the work, the increase in TGO thickness in the range of 75 ÷ 90 µm reduced the adhesion strength of 20YSZ and NiAl coatings due to the increase in residual compressive stress at the interface of these coatings when expanding the TGO thickness. In addition, because of the mismatch in properties between the ceramic, TGO, and metal, the formation of cracks at or near the TGO layer by the pull strength in the adhesion testing process can then easily propagated at the boundary leading to the fracture of the ceramic coating. This is the reason why the damaged position in the adhesion test moved from the interface of the NiAl coating and the 310S steel substrate (for the exposed sample at 1000 °C for 8 hours) to the interface of the NiAl coating and the 20YSZ coating (for the samples with the longer thermal oxidation time).

Table 3. The adhesive strength of the coating versus the time of oxidation at 1000 °C.

The thermal oxidation time, hours	Adhesive strength, MPa
0	12.53
8	38.52
24	24.58
48	29.07
120	24.93
200	25.29

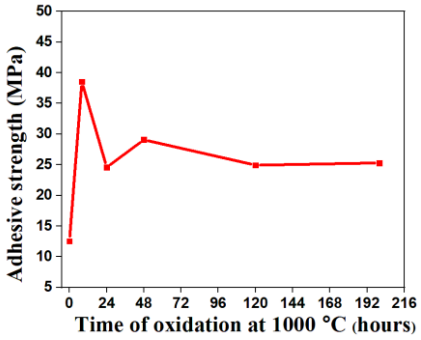

Figure 12. The adhesive strength of the coating versus the time of oxidation at 1000 °C.

4. CONCLUSIONS

In this study, the isothermal oxidation property of the 20YSZ/NiAl plasma coating system was investigated. Accordingly, the 20YSZ/NiAl coating system was undergone the thermal oxidation test at 1000 °C for 8, 24, 48, 120, and 200 hours in the air environment, and the following results were obtained:

- The 20YSZ/NiAl plasma coating system was not damaged after the exposure at 1000 °C for 200 hours.

- The porosity of the coating decreased with increasing the thermal oxidation time, reaching the lowest value of 9.8 % after 200 h of testing. It could be decreased by 62.3 % compared to the initial coating. The TGO formed at the interface of the NiAl bond coat and the 20YSZ top coat had the lowest thickness of 53.6 µm after holding at 1000 °C for 8 hours and the highest value of 90.2 µm after exposure at 1000 °C for 200 hours. The growth rate of TGO layer thickness tended to slow down and stabilize for the isothermal oxidation time in a range of 24 ÷ 200 hours.

- The main phase component of the 20YSZ coating was thermally stable of the arkalite (ZrO_2) with the cubic crystal structure.

- The adhesion of the 20YSZ/NiAl coating system on the 310S steel substrate reached a value of about 12.53 MPa. This value was significantly improved after the sample was exposed at 1000 °C.

Acknowledgments. This study was financially supported by the Institute of Tropical Technology, Vietnam Academy of Science and Technology (2022).

CRediT authorship contribution statement. Pham Thi Ly: Writing–Review & Editing, Methodology, Investigation, Formal analysis. Nguyen Van Tuan: Conceptualization, Review. Nguyen Tuan Anh: Formal analysis. Pham Thi Ha: Investigation, Editing. Dao Bich Thuy: Formal analysis. Ly Quoc Cuong: Investigation. Vo An Quan: Formal analysis. Le Hai Dang: Formal analysis.

Declaration of competing interest. The authors declare that they have no known competing financial interests or personal relationships that could have appeared to influence the work reported in this paper.

REFERENCES

1. Miller R. A. - Thermal barrier coatings for aircraft engines: history and directions, J. Therm. Spray Technol. **6** (1) (1997) 35-42. https://doi.org/10.1007/BF02646310.
2. Bakan E., Vanben R. - Ceramic Top Coats of Plasma-Sprayed Thermal Barrier Coatings: Materials, Processes, and Properties, J. Therm. Spray Technol. **26** (2017) 992-1010. https://doi.org/10.1007/s11666-017-0597-7.
3. Cao X.Q., Vassen R., and Stoever D. - Ceramic Materials for Thermal Barrier Coatings, J. Eur. Ceram. Soc. **24** (1) (2004) 1-10. https://doi.org/10.1016/S0955-2219(03)00129-8.
4. Hasselman D. P. H., Johnson L. F., Bentsen L. D., Syed R., Lee H. L., Swain M. V. - Thermal Diffusivity of Conductivity of Dense Polycrystalline ZrO_2 Ceramics: A Survey, Am. Ceram. Soc. Bull. **66** (1987) 799-806.
5. Pawlowski L., Lombard D., and Fauchais P. - Structure–Thermal Properties Relationship in Plasma Sprayed Zirconia Coatings, J. Vac. Sci. Technol. A **3** (6) (1985) 2494-2500.
6. Vourlias G., Pistofidis N., Chanliambalias D., Tsiaoussis I., Stergioudis G., Polychroniadis E. K. - A preliminary study of the structure and the corrosion performance of plasma sprayed YSZ coatings, J. Optoelectron. Adv. Mater. **9** (6) (2007) 1660-1664.
7. Fauchais P., Vardelle M., Goutier S. - Latest researches advances of plasma spraying: From splat to coating formation, J. Therm. Spray Technol. **25** (2016) 1534-1553. https://doi.org/ 10.1007/s11666-016-0435-3.
8. Muttera M., Mauera G., Mückea R., Guillon O., Vaßen R. - Correlation of splat morphologies with porosity and residual stress in plasma-sprayed YSZ coatings, Surf. Coat. Technol. **318** (2017) 157-169. https://doi.org/10.1016/j.surfcoat.2016.12.061.
9. Gan J. A., Berndt C. C. - Quantification and taxonomy of pores in thermal spray coatings by image analysis and stereology approach, Metall. Mater. Trans. A **44** (2013) 4844-4858. https://doi.org/10.1007/s11661-013-1818-4.
10. Sobhanverdi R., Akbari A. - Porosity and microstructural features of plasma sprayed Yttria stabilized Zirconia thermal barrier coatings, Ceram. Int. **41** (10) (2015) 14517-14528. https://doi.org/10.1016/j.ceramint.2015.07.102.
11. Xiaofeng Z., Kesong Z., Huantao C., Tao H., Jinbing S., Min L. - Properties of Thermal Barrier Coatings Made of Different Shapes of ZrO_2-7wt%Y_2O_3 Powders, Rare Met. Mater. Eng. **44** (6) (2015) 1301-1306. https://doi.org/10.1016/S1875-5372(15)30079-5.
12. Yu Z. X., Huang J. B., Wang W. Z., Wu L. - Deposition and properties of a multilayered thermal barrier coating, Surf. Coat. Technol. **288** (2016) 126-134. https://doi.org/10.1016/ j.surfcoat.2016.01.001.

13. Huang J., Wang W., Yu J., Wu L., Feng Z. - Effect of Particle Size on the Micro-cracking of Plasma-Sprayed YSZ Coatings During Thermal Cycle Testing, J. Therm. Spray Technol. **26** (2017) 755-763. https://doi.org/10.1007/s11666-017-0547-4.
14. Liu T., Luo X. T., Chen X., Yang G. J., Li C. X., Li C. J. - Morphology and Size Evolution of Interlamellar Two-Dimensional Pores in Plasma-Sprayed $La_2Zr_2O_7$ Coatings During Thermal Exposure at 1300 °C, J. Therm. Spray Technol. **24** (2015) 739-748. https://doi.org/10.1007/ s11666-015-0236-0.
15. Giolli C., Scrivani A., Rizzi G., Borgioli F., Bolelli G., Lusvarghi L. - Failure Mechanism for Thermal Fatigue of Thermal Barrier Coating Systems, J. Therm. Spray Technol. **18** (2009) 223-230. https://doi.org/10.1007/s11666-009-9307-4.
16. Rajendran R. - Gas turbine coatings – an overview, Eng. Fail. Anal. **26** (2012) 355-369. https://doi.org/10.1016/j.engfailanal.2012.07.007.
17. Liu X. Y., Wang X. Z., Javed A., Zhu C., Liang G. Y. - The effect of sintering temperature on the microstructure and phase transformation in tetragonal YSZ and LZ/YSZ composites, Ceram. Int. **42** (2) (2016) 2456-2465. https://doi.org/10.1016 /j.ceramint.2015.10.046.
18. Keyvani A., Saremi M., Sohi M. H., Valefi Z. - A comparison on thermomechanical properties of plasma-sprayed conventional and nanostructured YSZ TBC coatings in thermal cycling, J. Alloys Compd. **541** (2012) 488-494. https://doi.org/10.1016/ j.jallcom.2012.06.062.
19. Jamali H., Mozafarinia R., Razavi R. S., Ahmadi-Pidani R., Loghman-Estarki M. R. - Fabrication and Evaluation of Plasma-Sprayed Nanostructured and Conventional YSZ Thermal Barrier Coatings, Curr. Nanosci. **8** (2012) 402-409.
20. Foroushani M. H., Shamanian M., Salehi M., Davar F. - Porosity analysis and oxidation behavior of plasma sprayed YSZ and YSZ/$LaPO_4$ abradable thermal barrier coatings, Ceram. Int. **42** (14) (2016)15868-15875. https://doi.org/10.1016/j.ceramint.2016.07.057.
21. Doleker K.M., Ozgurluk Y., Parlakyigit A.S., Ozkan D., Gulmez T., Karaoglanli A. C. - Oxidation Behavior of NiCr/YSZ Thermal Barrier Coatings (TBCs), Open Chem. **16** (2018) 876-881. https://doi.org/10.1515/chem-2018-0096.
22. Yang G. J., Chen Z. L., Li C. X., and Li C. J. - Microstructural and Mechanical Property Evolutions of Plasma-Sprayed YSZ Coating During High-Temperature Exposure: Comparison Study Between 8YSZ and 20YSZ, J. Therm. Spray Tech. **22** (2013) 1294-1302. https://doi.org/10.1007/s11666-013-9986-8.
23. Huang J., Chu X., Yang T., Fang H., Ye D., Wang W., Zhang X., Sun W., Huang R., Li C. J. - Achieving high anti-sintering performance of plasma-sprayed YSZ thermal barrier coatings through pore structure design, Surf. Coat. Technol. **435** (2022) 128259. https://doi.org/ 10.1016/j.surfcoat.2022.128259.
24. Paraschiv A., Banu A., Doicin C., Ionica I. - Iso thermal oxidation behavior of plasma sprayed conventional and nanostructure YSZ thermal barrier coatings, U.P.B. Sci. Bull., B **82** (2) (2020) 163-174.
25. Li G., Xie H., Yang GJ., Liu G., Li C. X., Li C. J. - A comprehensive sintering mechanism for TBCs-part I: an overall evolution with two-stage kinetics, J. Am. Ceram. Soc. **100** (5) (2017) 2176-2189. https://doi.org/10.1111/jace.14784.

26. Cipitria A., Golosnoy I., Clyne T. - A sintering model for plasma-sprayed zirconia TBCs. Part I: free-standing coatings, Acta Mater. **57** (4) **(2009)** 980-992. https://doi.org/ 10.1016/j.actamat.2008.10.024.
27. Arantes T. M., Mambrini G. P., Stroppa D. G., Leite E. R., Longo E., Ramirez A. J., and Camargo E. R. - Stable colloidal suspensions of nanostructured zirconium oxide synthesized by hydrothermal process, J. Nanopart. Res. **12** (2010) 3105-3110. https://doi.org/10.1007/ s11051-010-9906-5.
28. William D., Callister J. R., David G. R. - Fundamentals of materials science and engineering: An integrated approach, Wiley, New York. 2012.
29. Behbahani A., Rowshanzamir S., Esmaeilifar A. - Hydrothermal synthesis of zirconia nanoparticles from commercial zirconia, Procedia Eng. **42** (2012) 908-917. https://doi.org/ 10.1016/j.proeng.2012.07.483.